J Mater Sci (2008) 43:4631–4643
DOI 10.1007/s10853-008-2669-z

Photographing impact of plasma-sprayed particles on rough substrates

André McDonald · Sanjeev Chandra · Christian Moreau

Received: 22 December 2007 / Accepted: 21 April 2008 / Published online: 13 May 2008

Abstract Plasma-sprayed nickel and molybdenum particles (~55 μm diameter) were photographed during spreading on silicon wafers that were patterned with micron-sized columns to make a textured rough surface. Impact on grit-blasted glass was also studied. The surfaces were maintained at either room temperature or at 350 °C. As the droplets approached the surface they were sensed by a photodetector and, after a known delay, a fast charge-coupled device (CCD) camera was triggered to capture time-integrated images of the spreading splat. A rapid two-color pyrometer was used to collect the thermal radiation from the spreading particles to record the evolution of their temperature and calculate splat cooling rates. It was found that micron-sized columns on the textured surfaces impeded fluid flow during spreading of splats, promoting splashing. When the column height was on the order of the splat thickness, increasing the space between each column increased the splat cooling rate as the columns penetrated into the liquid splat, providing a larger surface area for heat transfer. On the grit-blasted glass surfaces it was found that as the surface roughness increased, the maximum spread diameters of the molten droplets decreased, while the splat cooling rates increased. Impact on non-heated and heated roughened glass with similar roughness values produced splats with approximately the same maximum spread diameters, skewed morphologies, and cooling rates. On smooth glass, the splat morphologies were circular, with large maximum spread diameters and smaller cooling rates on non-heated smooth glass. An established model was used to estimate the splat-substrate thermal contact resistances. On highly roughened glass, the thermal contact resistance decreased as the glass roughness increased, suggesting that splat-substrate contact was improved as the molten metal penetrated the spaces between the large asperities.

A. McDonald (✉)
Department of Mechanical Engineering, University of Alberta, Edmonton, AB, Canada T6G 2G8
e-mail: andre.mcdonald@ualberta.ca

S. Chandra
Center for Advanced Coatings Technology, Department of Mechanical and Industrial Engineering, University of Toronto, Toronto, ON, Canada M5S 1A4

C. Moreau
National Research Council Canada, Industrial Materials Institute, Boucherville, QC, Canada J4B 6Y4

Introduction

Extensive studies have been conducted to photograph and analyze the spreading and fragmentation of plasma-sprayed particles on smooth surfaces. Mehdizadeh et al. [1] and Shinoda et al. [2] have shown, through in situ images, that significant disintegration of plasma-sprayed ceramic and metal particles occurs during spreading on non-heated glass. These studies were extended to show that the temperature of the substrate influences the extent of splashing and the splat morphology [3, 4]. It was shown that increasing the substrate temperature reduced the occurrence of splashing and produced disk-like splats [3]. In other cases, finger-like splash projections were observed on the splat periphery on the heated surfaces [4]. Droplet in-flight velocity was also shown to influence splat morphology and the occurrence of fragmentation. Aziz and Chandra [5] have observed the impact and spreading of molten tin droplets on mirror-polished stainless steel. For low speed impact (less than 4 m/s) on steel samples held at

room temperature, as the droplet impact velocity was increased, the maximum diameter of the splat increased, and was accompanied by significant splashing. Scanning electron microscope (SEM) images of molybdenum particles after high velocity impact (80–200 m/s) on polished 304L stainless steel also showed significant splashing at higher impact velocities [6].

Impact velocity was only one parameter that induced fragmentation and splashing during low velocity impact studies. Shakeri and Chandra [7] showed that the substrate surface roughness plays an integral role in promoting splat fragmentation and splashing. It was observed that on rough stainless steel coupons, splashing of molten tin droplets increased as the substrate surface roughness increased from 0.06 to 0.56 μm. The morphology of the final splat became complex and non-circular as the surface roughness was increased. Increasing the surface roughness to 3.45 μm suppressed splashing. It was suggested that increasing the roughness increased the thermal contact resistance between the splat and substrate, which delayed the onset of splat solidification and reduced splashing [7]. However, no splat temperature or cooling rates were measured to confirm this hypothesis.

Studies have been conducted to measure the thermal contact resistance between the spreading splat and rough surfaces. Heichal and Chandra [8] measured the thermal contact resistance between 4 mm diameter droplets and rough solid metal plates. With the substrate temperature variation under the spreading droplet, an analytical model was used to find that thermal contact resistances varied between 10^{-7} and 3×10^{-6} m^2 K/W when the droplet impact velocity was between 1 and 3 m/s. However, in plasma spraying, droplet sizes are on the order of 100 μm or less and reach velocities on the order of 100 m/s. To that end, Bianchi et al. [9] estimated the thermal contact resistance between plasma-sprayed zirconia and stainless steel by adjusting assumed thermal contact resistance values in a numerical model in order to match the experimental cooling rate of zirconia with that of a numerical simulation.

Fully understanding the mechanisms of the spreading of the liquid in the microgrooves and microasperities of a rough surface can be challenging. Sivakumar et al. [10] studied the impact of water droplets with 3.0 mm diameters and velocities lower than 2 m/s on textured stainless steel. The textured stainless steel had regular patterns of columns with heights that varied from 0.1 to 0.5 mm. It was found that increasing the Weber number and impact velocity allowed the splat liquid to penetrate the spaces between the columns. The columns perturbed the fluid during spreading and induced splashing, to form liquid jets and satellite droplets. Shinoda et al. [11] extended the study of particle spreading on rough surfaces to plasma-sprayed alumina on micropatterned quartz glass. It was found that an arithmetic mean roughness as low as 0.5 μm was sufficient to perturb the fluid flow and induce gas entrapment beneath the splat. Although investigations have been conducted to study particle spreading on prefabricated textured surfaces, limited information is available for impact on more realistic grit-blasted roughened surfaces.

The objectives of this study were to: (1) photograph plasma-sprayed nickel and molybdenum particles spreading on textured silicon wafers with varying column heights and inter-columnar spacing; (2) photograph molybdenum splats on grit-blasted glass substrates; (3) use two-color pyrometry to measure the cooling rates of the splats; and (4) determine the effect of micrometer average surface roughnesses on splat morphologies and cooling rates.

Experimental methods

In situ images of plasma-sprayed particles on grit-blasted glass and textured silicon wafers (General Electric Global Research, Niskayuna, NY, USA) were captured by using the assembly described by McDonald et al. [12]. Figure 1 shows a schematic diagram of the experimental setup. A SG100 plasma torch (Praxair Surface Technologies, Indianapolis, IN, USA) was used to melt and accelerate molybdenum (SD152, Osram Sylvania Chemical and Metallurgical Products, Towanda, PA, USA) and nickel (56C-NS, Sulzer Metco, Westbury, NY, USA) powder particles, sieved to diameters lying between 38 and 63 μm, with an average diameter of 55 μm. The powder feed rate was less than 1 g/min.

Some of the substrates were patterned silicon wafers that had regular patterns of square columns with varying heights and distance between the columns. Figure 2 shows details of the geometrical parameters of the textured silicon wafers. In the figure, l is the height of the column, b is the space between the columns, and w is the width of the column. Figure 3 shows a scanning electron microscope (SEM) image of a typical textured silicon wafer used in this study. The column width (w) on all the wafers was 4 μm. The height of the columns (l) was either 1 or 3 μm; the space between the columns (b) was either 1 or 5 μm. All wafer samples were heated to 350 °C during spraying by placing them in a copper substrate holder that included cartridge heaters (Omega, Laval, QC, Canada).

Other substrates were smooth or roughened glass slides. The average roughnesses (R_a) of the three roughened slides were 1.25, 2.75, and 7.0 μm. Some glass slide samples were heated to 370 °C during spraying. The glass slides with $R_a = 1.25$ μm and $R_a = 2.75$ μm were high-quality ground glass roughened with 120-grit and 220-grit sandblast, respectively (Edmund Optics, Barrington, NJ, USA). The glass slides with $R_a = 7.0$ μm were microscope slides

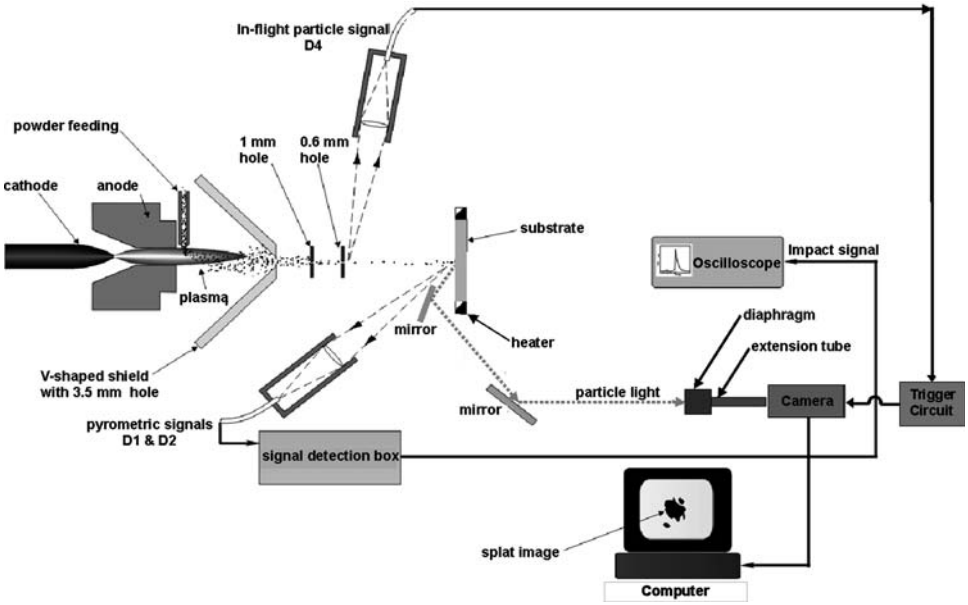

Fig. 1 Schematic of the experimental assembly

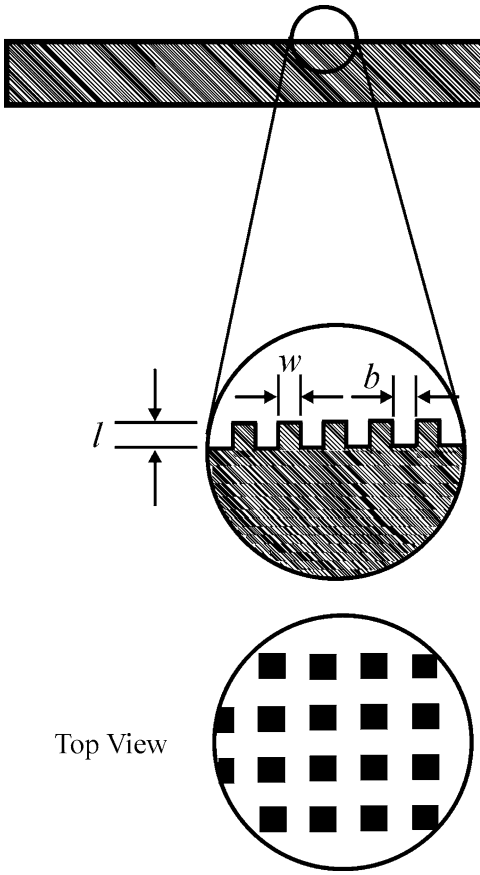

Fig. 2 Geometrical parameters of the textured silicon wafers

(Fisher Scientific, Pittsburgh, PA, USA) that were grit-blasted with black silicon carbide. Figure 4 shows confocal microscope images of the topology of the roughened surfaces. Due to the large roughness of the slides with $R_a = 7.0$ μm, clear images of the surface were difficult to

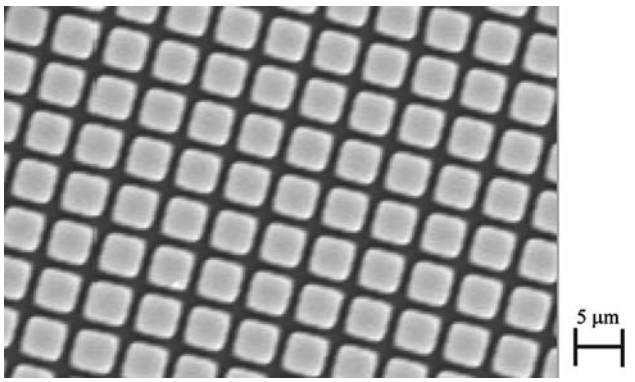

Fig. 3 SEM image of a typical textured silicon wafer

capture. The surface roughness was measured with a surface roughness gage (Pocketsurf, Federal Products, Co., Providence, RI, USA).

The plasma torch was operated with a voltage of 35 V and a current of 700 A. The plasma gas mixture was argon at a flow rate of 50 L per minute (LPM) and helium at 24.5 LPM. The torch was passed rapidly across the substrates. In order to protect the substrate from an excess of particles and heat, a V-shaped shield was placed in front of the torch. This V-shaped shield had a 3.5 mm hole through which particles could pass. To reduce the number of particles landing on the substrate, two additional barriers were placed in front of the substrate, the first of which had a 1 mm hole and the second, a 0.6 mm hole. All the holes were aligned to permit passage of the particles with a horizontal trajectory (Fig. 1).

After exiting the third barrier and just before impacting the substrate, the thermal radiation of the particles was measured with a fast two-color pyrometry system (D_1 and

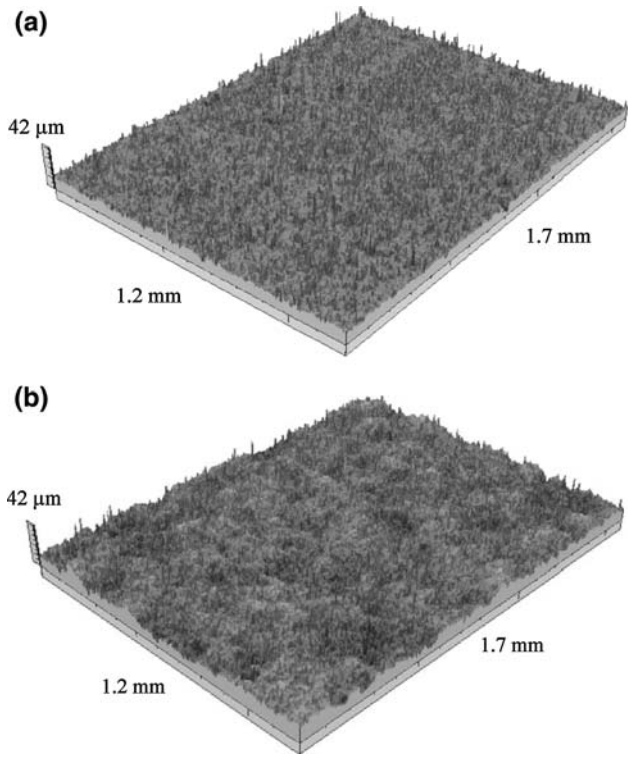

Fig. 4 Confocal microscope images of the topology of glass slides roughened to (**a**) 1.25 μm and (**b**) 2.75 μm

D_2 sensor). Mehdizadeh et al. [1] have described this system in detail. Other investigators have used this method to measure the in-flight velocity and temperature of plasma-sprayed droplets as well as the splat cooling rate and flattening time after impact [13, 14]. The system included an optical sensor head that consisted of a custom-made lens, which focused the collected radiation, with a 0.44 magnification, onto an optical fiber with an 800 μm core [1]. This optical fiber was covered with an optical mask that was opaque to near infrared radiation, except for three slits. Two of the slits, with dimensions of 30 μm by 150 μm and 30 μm by 300 μm, were used to detect the thermal radiation of the in-flight particles. The radiation was used to calculate the temperature and velocity of the in-flight particles [1, 15]. The largest slit, measuring 150 μm by 300 μm, was used to collect thermal radiation of the particle as it impacted and spread on the substrate. With the thermal radiation from this slit, the splat temperature, diameter, and cooling rate were calculated at 100 or 200 ns intervals after the impact. The droplet average in-flight velocity was calculated by dividing the known distance between the centers of the two smaller slits by the measured time of flight. The distance between the centers of the two small slits was approximately 65 μm.

The collected thermal radiation was transmitted through the optical fiber to a detection unit that contained optical filters and two photodetectors. The radiation beam was divided into two equal parts by a beam splitter. Each signal was transmitted through a band pass filter with wavelength of either 785 or 995 nm and then detected using a silicon avalanche photo detector (model C30817, RCA, Durant, OK, USA). The photo detector had a response time smaller than 0.1 μs [16]. The ratio of the radiation intensity at these wavelengths was used to calculate the particle temperatures with an accuracy of ±100 °C [15]. The signals were recorded and stored by a digital oscilloscope.

A 12-bit CCD camera (QImaging, Burnaby, BC, Canada) was used to capture images of the spreading particles. The electronic shutter of the camera was triggered to open by a signal from the D_4 sensor (Fig. 1). The camera was attached to a 30 cm long optical extension tube that was connected to a diaphragm (Tominon, Waltham, MA, USA). The diaphragm included a lens with a 135-mm focal length and an *f*-stop from 4.5 to 32. The diaphragm was set to an *f*-stop of 16, so that the diameter of the opening was 8.4 mm. In order to photograph the in-flight particles and the splats, the shutter of the camera was opened for about 500 μs, with no added illumination. This produced single, time-integrated images of the splats. The images captured by the camera were then digitized by a frame grabber and recorded on a personal computer.

Results and discussion

Impact on textured silicon wafers

Plasma-sprayed nickel and molybdenum particles impacted samples of textured silicon wafers. The wafers were held at 350 °C during spraying. The nickel particles were sprayed on silicon wafers with columns having heights of 1 μm and with inter-columnar spaces measuring either 1 or 5 μm. The molybdenum particles were sprayed on silicon wafers with columns having heights of 3 μm and with inter-columnar spaces measuring either 1 or 5 μm. The in-flight velocity and temperature of the nickel particles were 70 ± 2 m/s and 2,280 ± 30 °C, respectively; for molybdenum, they were 80 ± 2 m/s and 2,990 ± 35 °C, respectively. For nickel, 25 samples were collected for the average; for molybdenum, it was 20. The average in-flight diameter (D_o) was 55 μm, and was a weighted average obtained after particle size analysis. The standard error of the mean, calculated by dividing the standard deviation by the square-root of the number of samples [17], is shown with the averages. The standard errors of the mean will be reported with the averages of all other parameters mentioned in this study.

Figure 5 shows scanning electron microscope (SEM) images of plasma-sprayed nickel splats after spreading and

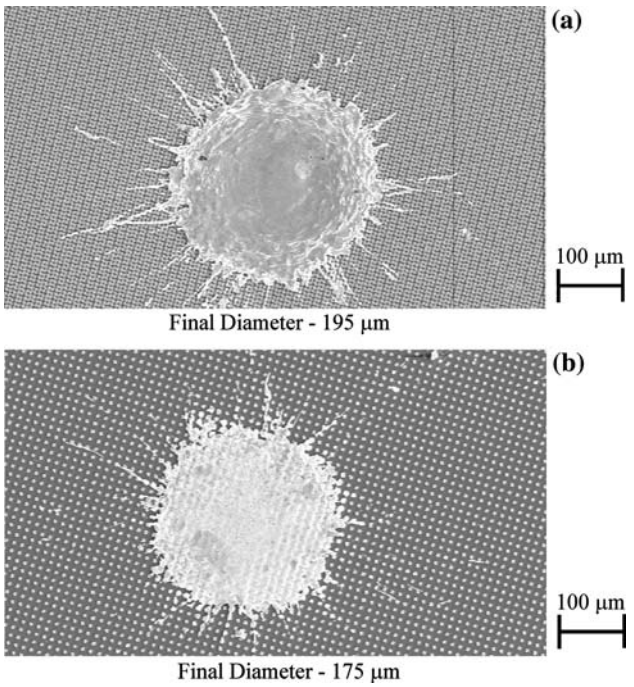

Fig. 5 Images of nickel splats after solidification on heated textured silicon wafers with 1 μm high columns and inter-columnar space of (**a**) 1 μm and (**b**) 5 μm

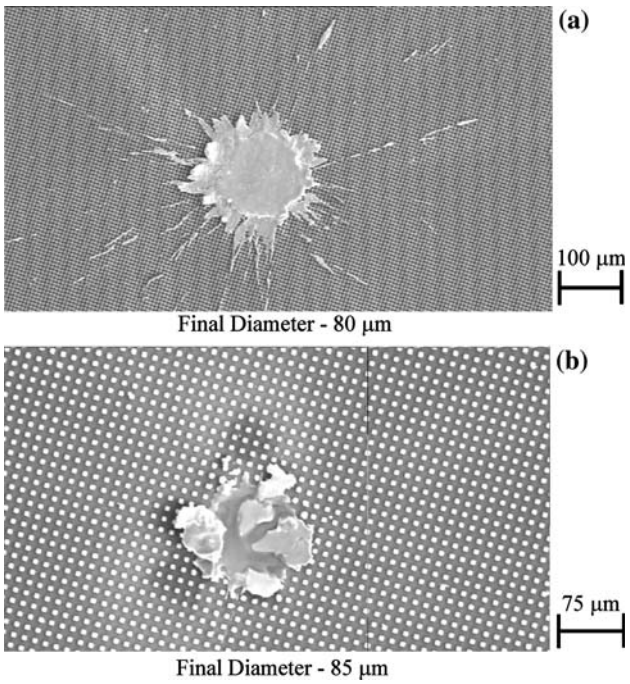

Fig. 6 Images of molybdenum splats after solidification on heated textured silicon wafers with 3 μm high columns and inter-columnar space of (**a**) 1 μm and (**b**) 5 μm

solidification on textured silicon wafers. Impact on silicon wafers having column heights of 1 μm and inter-columnar spaces of 1 μm (Fig. 5a) produced splats with slightly larger diameters (195 ± 10 μm) than those on wafers having the same column heights, but with inter-columnar spaces of 5 μm (Fig. 5b). The proximity of the columns on the silicon wafers of Fig. 5a influenced the splat thickness and the number of finger-like projections at the splat periphery—the splats appear thicker, with more splash-like projections at the periphery.

Molybdenum splats, after spreading and solidification, are shown in Fig. 6. On silicon wafers having column heights of 3 μm, the splats were smaller, with final diameters on the order of 80 μm. It is possible that the larger columns impeded the splat fluid during spreading, producing smaller splats. Smaller inter-columnar spaces (1 μm) produced splats with splash-like projections at the periphery (see Fig. 6a), while larger inter-columnar spaces (5 μm) resulted in splats with fragmented, flower-like morphologies (Fig. 6b). These morphologies are indicative of substrate melting [12, 18]. Substrate melting typically occurs when molybdenum spreads and solidifies on metals [18], and is enhanced by improved contact between the splat and substrate. With larger inter-columnar spaces, the molybdenum splats were probably in contact with a larger surface area on the substrate, promoting substrate melting (Fig. 6).

The influence of the column heights on the splat morphology was more clearly observed in images captured in situ during spreading. Figure 7 shows time-integrated images of nickel (Fig. 7a and b) and molybdenum splats (Fig. 7c and d) on textured silicon wafers. The maximum splat diameter (D_{max}) was taken as the maximum splat extent in the integrated images. The comet-like streak in the images represents the path of the in-flight particle. Table 1 shows the average maximum spread factors of the splats. The maximum spread factor (ξ_{max}) is defined as the ratio of the maximum splat diameter and the in-flight particle diameter. The ImageJ imaging software (National Institutes of Health, Bethesda, MD, USA) was used to estimate the splat area, A, which permitted calculation of the maximum spread diameter, $D_{max} = \sqrt{4A/\pi}$.

Impact of nickel on silicon wafers with columns having heights of 1 μm produced splats at their maximum extent with circular morphology (Fig. 7a and b). This morphology is similar to those observed on heated, smooth surfaces [3]. This suggests that on textured rough surfaces, column heights of 1 μm will not significantly affect the splat morphology. Splashing is more pronounced on the silicon wafers with an inter-columnar spacing of 5 μm (Fig. 7b) than on those with columns spaced 1 μm apart (Fig. 7a). Due to the proximity of the columns, the splats probably flowed on top of the columns without penetrating the spaces between the columns significantly. Increasing the space between the columns from 1 to 5 μm allowed the splats to penetrate and wet the spaces between the columns. However, the columns may act as an impediment to flow

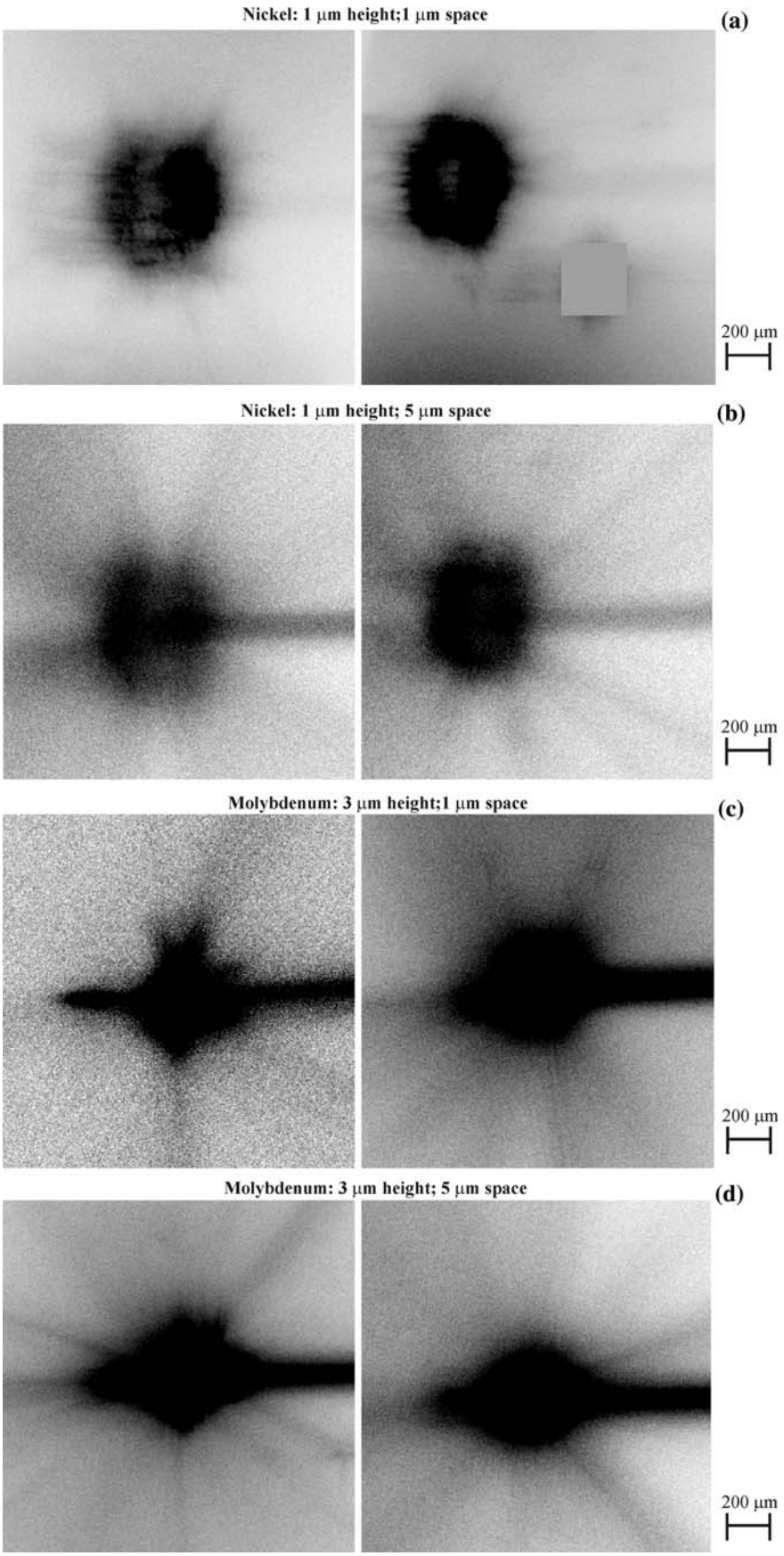

Fig. 7 Integrated images of (**a** and **b**) nickel and (**c** and **d**) molybdenum splats during spreading on textured silicon wafers

Table 1 Average maximum spread factors (ξ_{max}), cooling rates, total splat-substrate contact areas, and thermal contact resistances of nickel and molybdenum splats on textured silicon wafers

Particle	Nickel		Molybdenum	
Silicon wafer columns	1 μm height; 1 μm space	1 μm height; 5 μm space	3 μm height; 1 μm space	3 μm height; 5 μm space
ξ_{max}	7.2 ± 0.3	6.3 ± 0.3	5.9 ± 0.2	5.7 ± 0.2
D_o (μm)	50.1 ± 2.8	59.3 ± 3.3	57.6	58.9
Cooling rate (K/s ($\times 10^{-7}$))	9.0 ± 1.5	13.5 ± 1.4	9.2 ± 2.0	4.1 ± 0.7
Contact area (μm^2)	102,195	109,620	199,555	95,085
$R_c/A_{contact}$ (K/W)	55 ± 7	20 ± 2	40 ± 9	125 ± 17

during spreading, reducing the splat size and inducing splat splashing. Due to blocking of the fluid by the columns when the inter-columnar spaces are 5 μm, the maximum spread factor was 15% smaller than that on the wafers where the inter-columnar spaces were 1 μm (Table 1). Fluid jetting was also pronounced on the wafers where the inter-columnar spaces were 5 μm (Fig. 7b).

On the silicon wafers where the column heights were 3 μm, splat distortion at the maximum extent was more pronounced (Fig. 7c and d). Sivakumar et al. [10] have shown that asperity heights on roughened surfaces that are comparable to or much larger than the thickness of the liquid splat will have more pronounced effects on the spreading process. On the wafers in this study, the average thickness of the nickel and molybdenum splats at the maximum extent was on the order of 1 μm. As the splat spread and the thickness decreased, the columns were able to impede the fluid at certain points along the periphery. The rest of the fluid jetted through the spaces between the columns, producing a skewed morphology (Fig. 7c and d). Raessi et al. [19] have shown, with computer simulations, that alumina droplets spreading and solidifying on patterned surfaces with column heights of 3 μm will produce significant splat distortion and skewed morphology.

Figures 5–7 have shown that, in addition to splat morphology changes, the heights and inter-columnar spaces on the wafers also influence the occurrence of finger-like projections at the splat periphery. Pershin et al. [20] and Dhiman et al. [21] have suggested that large splat cooling rates during spreading will induce fingering at the splat periphery. The larger cooling rates increase splat solidification, and the solidified portions of the splat act as impediments to flow of the remaining liquid portions of the splat, inducing finger-like jetting. Table 1 shows the average cooling rates of nickel and molybdenum splats on textured silicon wafers. Two-color pyrometry was used to measure the temperature evolution of splats during spreading. Cooling rates were obtained from temperature measurements, as described earlier [3, 12, 21]. Typical splats of nickel (Fig. 5) and splats of molybdenum on the silicon wafers with inter-columnar spaces of 1 μm (Fig. 6a) exhibit cooling rates larger than 9.0×10^7 K/s. These splats all have finger-like projections protruding from their peripheries. For molybdenum splats on silicon wafers with inter-columnar spaces of 5 μm, the cooling rates were lower, and on the order of 4×10^7 K/s. No finger-like projections were observed at the peripheries of these splats (see Fig. 6b).

cIncreased cooling rates imply that physical contact between the splat and substrate is improved, and that the splat-substrate contact area is larger [3]. To test this hypothesis, a simple model was developed to estimate the total splat-substrate contact area on the textured silicon wafers. The total contact area was based on the splat diameter at the maximum spread extent ($D_{max} = \xi_{max} D_o$) (see Table 1).

The total surface area per repeating unit of columns on the textured wafer (A_{total}) is the sum of the total surface area of a column (A_{column}) and the total surface area of the inter-columnar space (A_{space}):

$$A_{total} = A_{column} + A_{space}. \quad (1)$$

The total surface area of a column is

$$A_{column} = w^2 + 4(l \times w). \quad (2)$$

The total surface area in the inter-columnar space of a repeating unit on the textured surface is

$$A_{space} = 2(b \times w) + b^2. \quad (3)$$

Figure 2 defines the parameters shown in Eqs. 1–3 above. Substituting Eqs. 2 and 3 into Eq. 1 gives the total surface area per repeating unit as

$$A_{total} = w^2 + 4(l \times w) + 2(b \times w) + b^2. \quad (4)$$

The total number of repeating units covered by the splat area is

$$u = \frac{\pi D_{max}^2}{4(w+b)^2}, \quad (5)$$

where u is the number of repeating units beneath the splat. The total splat-substrate contact area ($A_{contact}$) on the textured silicon wafer is

$$A_{contact} = A_{total} \times u = \left[w^2 + 4(l \times w) + 2(b \times w) + b^2\right] \times \frac{\pi D_{max}^2}{4(w+b)^2}. \quad (6)$$

Figure 8 shows images of plasma-sprayed nickel after focused ion beam (FIB) milling. Figure 8a shows that on

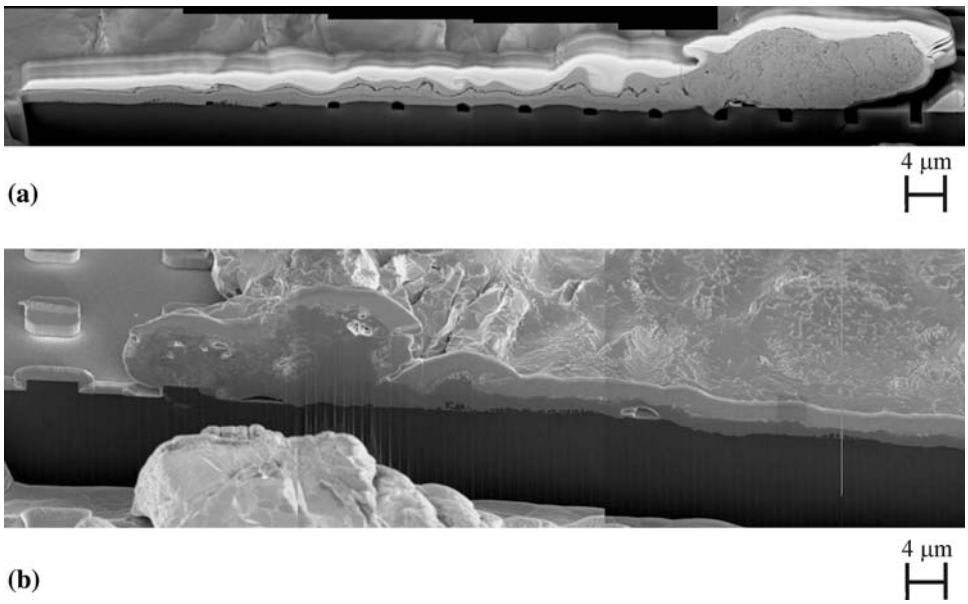

Fig. 8 SEM images of nickel splats on textured silicon wafers with 1 μm high columns and inter-columnar space of (**a**) 1 μm and (**b**) 5 μm after focused ion beam (FIB) milling

textured silicon wafers where the column heights were 1 μm and the inter-columnar space was 1 μm, splat liquid penetration into the inter-columnar spaces was significantly restricted. As a result, it was assumed that on this surface, the column height, l, was zero. Total splat penetration is observed in Fig. 8b.

Table 1 shows estimates of the total splat-substrate contact areas. For nickel, the contact area is larger on the textured silicon wafers where the inter-columnar space was 5 μm than on those where the inter-columnar space was 1 μm. Due to the larger splat-substrate contact area, the cooling rate was larger (see Table 1) and the splats appear thinner (see Fig. 5).

For molybdenum, the contact area was larger on the textured silicon wafers where the inter-columnar space was 1 μm than on those where the inter-columnar space was 5 μm. The large column heights (3 μm) acted as an impediment to fluid flow in both cases, restricting the size and the total splat-substrate contact areas (Table 1). However, the larger number of columns in contact with the splat on the silicon wafers where the inter-columnar space is 1 μm doubled the splat cooling rate (see Table 1). On this surface, the columns acted as fins that penetrated the splat and promoted the conduction of heat, increasing the splat cooling rate. The cross-sectional area ($A_C = \pi D_{max}^2/4$) of the molybdenum splats at the maximum extent on the silicon wafers where the inter-columnar space was 1 and 5 μm was 90,710 and 88,525 μm^2, respectively. However, Table 1 shows much larger splat-substrate contact areas, which indicates that the columns acted as fins and extended the heat transfer surface area. Figure 9 shows SEM images of molybdenum splats after FIB milling to expose the cross section of the splat. On the silicon wafer where the inter-columnar space is 1 μm, there were approximately 20 columns in contact with the splat; on the wafer where the inter-columnar space was 5 μm, there were approximately 10 columns in contact with the splat across the final diameter. Melting of the columns is also clearly visible, which confirms the flower-like morphology of the splat in Fig. 6b. It is well-known that substrate melting under the liquid splat may promote the occurrence of chemical reactions, leading to the formation of new materials with compositions that are intermediate between the pure states of the splat and substrate. Although the effects of chemical reactions on the spreading and cooling of the splats may be small, these effects are still not clearly understood.

The thermal contact resistance between the splat at the maximum spread extent and the textured silicon wafers can also be used as an indication of the degree of splat-substrate physical contact. Lower splat-substrate thermal contact resistances indicate improved physical contact; higher splat-substrate thermal contact resistances indicate reduced physical contact. A mathematical model was developed to estimate the thermal contact resistance between the splat and the textured wafers [22]. The splat cooling rate, thickness of the wafers, and the thermal properties of molten particles and solid wafers were used as inputs into the model. Table 1 shows that as the splat cooling rates and the total splat-substrate contact areas increased, the splat-substrate thermal contact resistance per unit total contact area ($R_c/A_{contact}$) decreased.

Liquid properties such as surface tension could have played a role in the penetration of the liquid into the inter-columnar spaces. However, Pasandideh-Fard et al. [23] have shown that for high velocity particle impact on flat

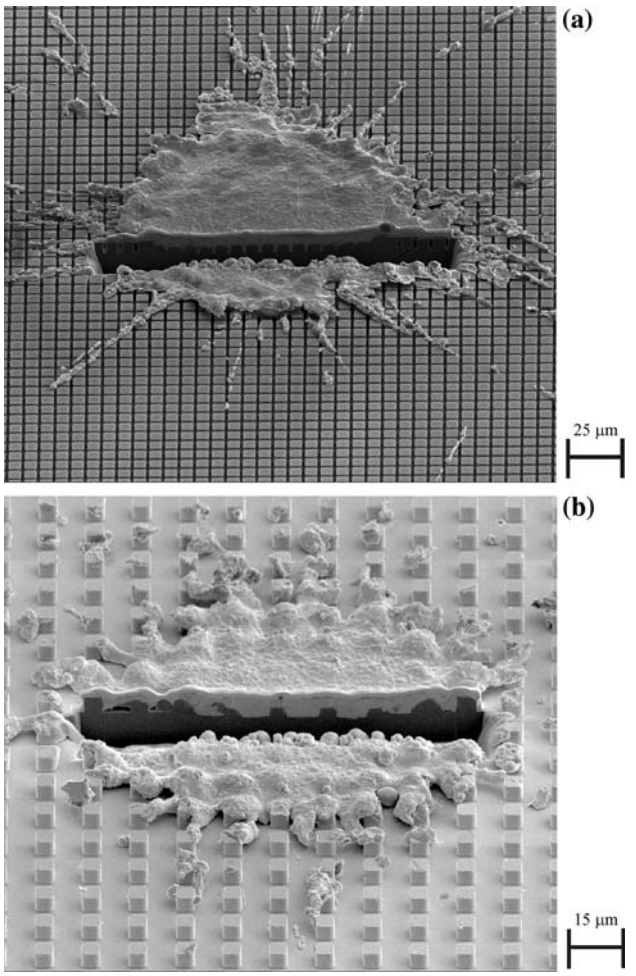

Fig. 9 SEM images of molybdenum splats on textured silicon wafers with 3 μm high columns and inter-columnar space of (**a**) 1 μm and (**b**) 5 μm after focused ion beam (FIB) milling

surfaces, surface tension effects are negligible during spreading of the splat. It was assumed that the properties of the droplets did not affect the penetration of liquid between the columns, and penetration was due to the high impact forces during impact. As a result, the results observed in this study were due mainly to the roughness of the surfaces.

Impact on grit-blasted glass slides

Studying the impact and spreading of plasma-sprayed particles on textured wafers with ordered columns that act as rough asperities provided a preliminary overview of impact on rough surfaces. Real surfaces have rough asperities that vary in size and morphology (see Fig. 4), and differ in their interaction with the spreading splat.

To study the interaction of real roughened surfaces with a molten, spreading particle, molybdenum was plasma-sprayed on smooth and roughened glass slides that were either held at room temperature or heated to 370 °C before spraying. The average in-flight velocity was 95 ± 1 m/s and the average in-flight temperature was 3,145 ± 10 °C. In this case, 102 samples were collected for the average. The average in-flight diameter (D_o) was also 55 μm. Figure 10 shows time-integrated images of different splats on glass slides. The glass slides were either smooth or roughened to 1.25, 2.75, or 7.0 μm. The average roughness of the smooth glass slides were measured with an atomic force microscope (Veeco Metrology Group, Santa Barbara, CA, USA) and was found to be approximately 1.0 nm. Due to the time-integrated nature of the images, the splats at the maximum extent can be clearly observed. Two comet-like streaks in the time-integrated images of plasma-sprayed nickel and molybdenum on silicon wafers were observed. These comet-like streaks were not present in the images captured on grit-blasted glass. On the non-heated glass slides, the average maximum spread factor ($\xi_{max} = D_{max}/D_o$) ranged from 5.8 to 8.6 (Fig. 10a), which represented maximum spread diameters between 320 and 475 μm. On the heated slides, the maximum spread factor range was 4.5–6.9 (Fig. 10b), which produced maximum spread diameters between 250 and 380 μm.

Impact on smooth (R_a = 1.0 nm) non-heated and heated glass produced round splats with average maximum diameters of 475 and 250 μm, respectively. Similar results were observed by Mehdizadeh et al. [1] and McDonald et al. [3]. Increasing the roughness of the glass surface produced splats at the maximum extent with highly distorted and random morphologies (Fig. 10). As the splat fluid flowed, the rough, random asperities that characterized the surfaces blocked the fluid and prevented flow into the crevices between asperities. Figure 10 shows that as the average roughness increased to values greater than 6 μm, the splat at the maximum extent became extremely distorted and fragmented as the large asperities blocked and broke the splat. Attempts were made to collect SEM images of the splats after spreading and solidification on the grit-blasted glass. No splats were observed on the surface. It is possible the splats fragmented without adhering to the surface.

Heating the smooth surfaces produced circular splats with noticeably smaller maximum diameters. This has been attributed to the vaporization of adsorbates and other contaminants from the surface [3, 24]. Due to the vaporization of adsorbates before impact and spreading, the physical contact between the droplets and the surface was significantly improved, which resulted in larger viscous dissipation losses and smaller splats [3]. Heating the roughened glass surfaces did not appear to follow the same trend observed on smooth surfaces. For each roughness value larger than 1.0 μm, the maximum spread factors were approximately equal on the heated and non-heated surfaces (see Fig. 10). The morphologies of the splats at

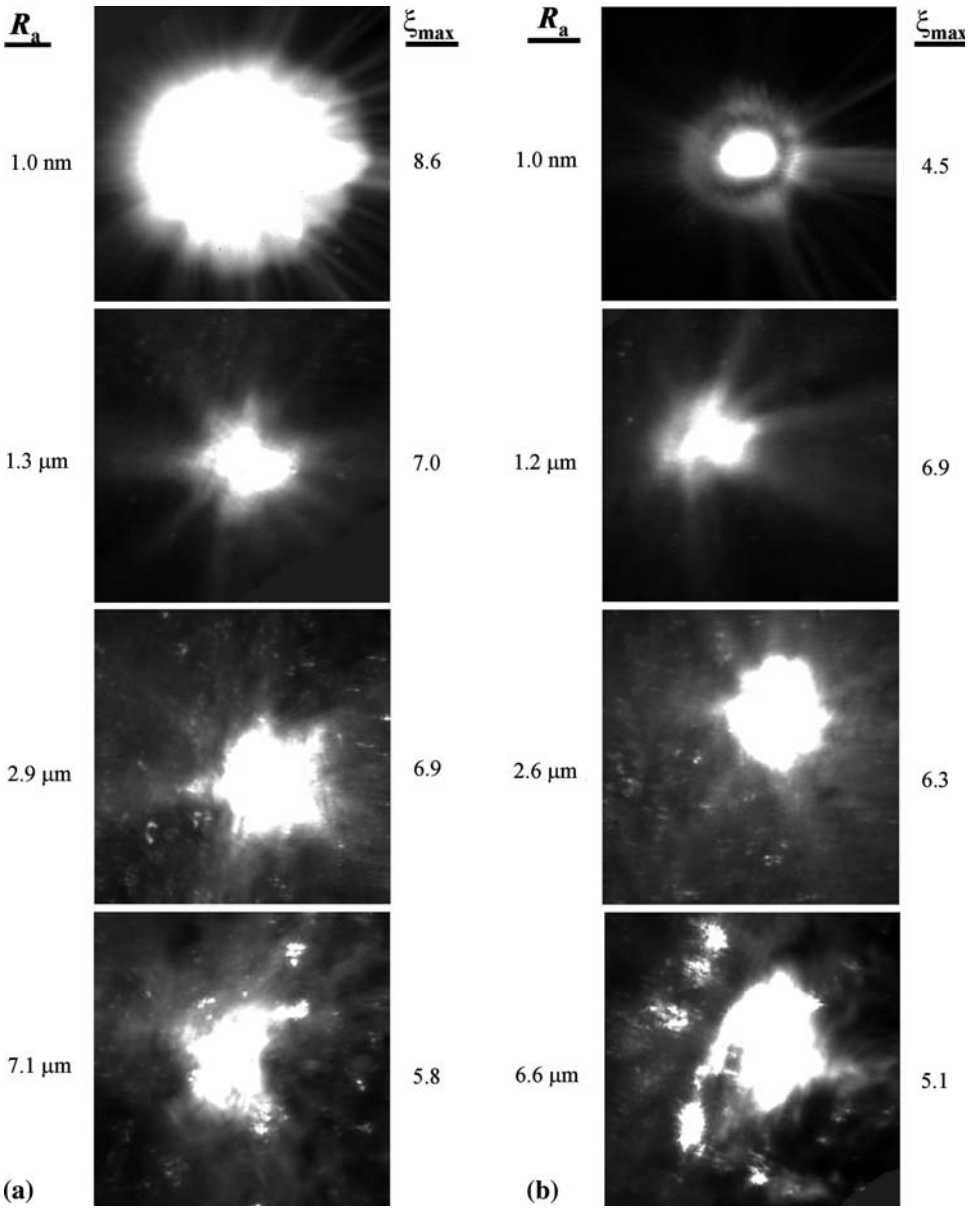

Fig. 10 Images of plasma-sprayed molybdenum splats during spreading on roughened glass (**a**) at room temperature and (**b**) heated to 370 °C

the maximum extent were also similar. In these cases, the rough asperities on the surfaces had greater influence on the splat size and morphology than the adsorbates. McDonald et al. [25] have recently shown that average roughness on a nanometer scale will have lesser influence on the splat morphology than adsorbates on the surface. However, the images and analysis shown in the present study suggest that average roughness on a micrometer scale will have a dominating effect on the splat size and shape.

Several studies have shown that on non-heated smooth surfaces, where the splats are significantly larger at the maximum spread extent, the splat cooling rates were smaller [3, 12, 25, 26]. On heated smooth surfaces, the splat cooling rates were larger, resulting in smaller splats at the maximum spread extent. The larger cooling rates on the heated surface were shown to be due to smaller thermal contact resistances between the splat and the surfaces [22].

Figure 11a shows the average splat cooling rates (dT/dt) on the glass substrates as a function of average roughness. Error bars depicting the standard error of the mean are shown. On smooth glass ($R_a = 1.0$ nm–0 μm), the cooling rate is two times larger on heated glass than on non-heated glass. Increasing the average roughness of the glass surface produced approximately equal splat cooling rates on the non-heated and heated surfaces. An increase in the average roughness of the glass slides produced large asperities that impeded the splat fluid flow, reducing spreading. Blocking the splat fluid from penetrating into surface cavities reduced the true contact area between the splat and the surface. As a result, Fig. 11a shows that the splat cooling

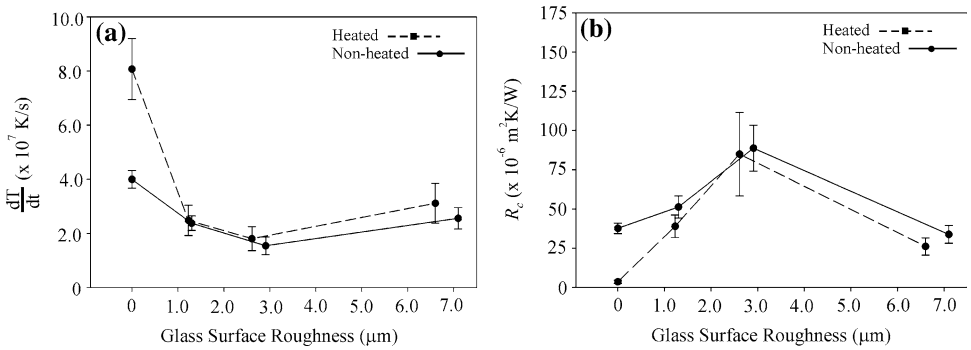

Fig. 11 (**a**) Splat cooling rates (d*T*/d*t*) and (**b**) thermal contact resistances (R_c) as a function of glass surface roughness

rate decreased significantly when the surface was roughened to 1.25 μm. Increasing the average roughness of the glass slides beyond 2.75 μm increased the splat cooling rate. At large R_a values, there were larger spaces between the asperities. This increased the physical contact between the liquid splat and the rough surface, increasing the splat cooling rate. Similar results were observed for plasma-sprayed nickel splats on textured silicon wafers when the inter-columnar space was increased from 1 to 5 μm (Table 1).

The thermal contact resistance between the splat and the substrate was estimated based on the splat cooling rate, the thickness of the glass slide samples (1–2 mm), and the thermal properties of molten molybdenum and solid glass slides as model inputs. Figure 11b shows a graph of the thermal contact resistance as a function of the glass surface roughness. Since the splat cooling rate decreased significantly when the glass average roughness was increased to 1.25 μm, the thermal contact resistance increased significantly. Increasing the glass average roughness beyond 2.75 μm resulted in a decrease in the splat-surface thermal contact resistance as the splat-substrate physical contact improved. With the exception of the smooth glass surfaces, thermal contact resistance on the non-heated and heated surfaces were close. On the smooth surfaces, thermal contact resistance was due to the presence of adsorbates. However, when large, micrometer-sized asperities are present on the surface, they create such a large thermal contact resistance that adsorbates create only a very small additional barrier. The contact resistance on heated and non-heated rough surfaces was, therefore, almost the same (Fig. 11b). Through photography and analysis, Syed et al. [27] also found that surface roughness and surface chemistry partially influenced splat morphology and spreading.

An analytical model was developed by Heichal and Chandra [7] to calculate the thermal contact resistance between molten metal droplets on roughened metal substrates. In this model, the surface roughness was assumed to be a series of half cylinders aligned next to each other. An expression for the thermal contact resistance was developed after it was assumed that the spreading splat was semi-infinite. The results from this model were generated for droplets impacting at low velocity compared to that of this study. This model was used to calculate the thermal contact resistance between the molybdenum splats and the glass surfaces in the present study. On smooth glass surfaces, where the average roughness was on the order of 1 nm, the predicted thermal contact resistances were on the order of 1×10^{-8} m^2 K/W. Increasing the average surface roughness to 1.25, 2.75, and 7.0 μm produced thermal contact resistances on the order of 3.5×10^{-7}, 8×10^{-7}, and 2×10^{-6} m^2 K/W, respectively. These thermal contact resistance values were more than an order of magnitude smaller than those reported in Fig. 11b. On the smooth glass surfaces, the thermal contact resistances predicted by the model of Heichal and Chandra [7] were more than two orders of magnitude smaller than those shown in Fig. 11b. These large differences were probably due to the assumption by Heichal and Chandra [7] of a surface topology consisting of a series of half-cylinders aligned next to each other, low velocities of the impacting droplet, and a semi-infinite spreading splat. In this study, the assumption of a semi-infinite splat would not apply in the determination of the thermal contact resistance because the splats were thin. Figure 12 shows a confocal microscope image of a typical roughened glass surface ($R_a = 2$ μm) at high magnification. The asperities on this

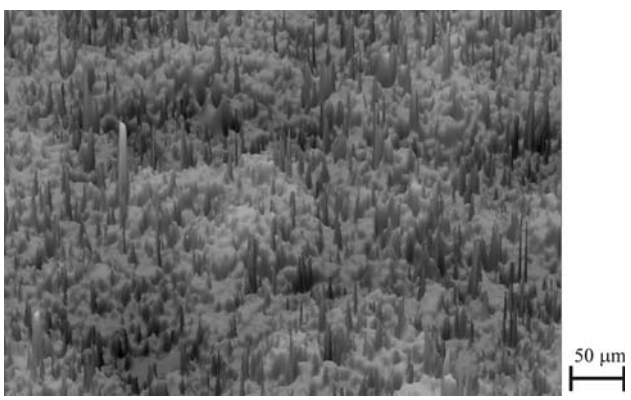

Fig. 12 Confocal microscope image of a typical roughened glass surface ($R_a = 2$ μm) at high magnification

real surface are pointed projections rather than a series of ordered half-cylinders. In addition, there may also be residual contaminants on the rough glass surfaces, not accounted for in the theory developed by Heichal and Chandra [7].

Conclusion

The influence of substrate roughness on splat morphology, splat cooling rates, and thermal contact resistances between the splat and substrate was studied. Plasma-sprayed nickel and molybdenum particles were photographed during spreading on silicon wafers that were patterned with micron-sized columns to make a textured rough surface. On wafers with column heights on the order of the splat thickness, the splats exhibited circular morphology; on wafers where the column heights were larger than the splat thickness, a skewed splat morphology was observed, since larger column heights impeded flow during spreading. The cooling rate, as calculated from two-color pyrometry, was used as a qualitative indicator of physical contact between the splat and the textured surfaces. On silicon wafers where the column heights were approximately equal to the splat thickness, increasing the inter-columnar space increased the cooling rate and when column heights were larger than the splat thickness, smaller inter-columnar spaces promoted splat cooling since many large columns acted as fins, protruding into the splat. SEM images captured after focused ion beam milling showed that twice as many columns penetrated the splat when the inter-columnar space was smaller.

A simple calculation was conducted to estimate the total splat-substrate contact area on the textured wafers. It was found that on wafers with small column heights, increasing the inter-columnar spaces, increased the total splat-substrate contact area. This was confirmed by the increased splat cooling rate on wafers with larger inter-columnar spaces. However, calculations showed that as the column heights increased, the total splat-substrate contact area increased as the inter-columnar space was decreased. This agreed well with the larger splat cooling rates observed on patterned surfaces with smaller inter-columnar spaces.

Impact on grit-blasted glass were also studied to provide results on random roughened surfaces. Plasma-sprayed molybdenum particles that impacted and spread on these surfaces formed splats that were highly distorted and smaller compared to those splats on smooth surfaces. The splat cooling rates decreased significantly when the glass surfaces were roughened to $R_a = 1.25$ μm, but increased as the average roughness increased beyond 2.75 μm. The thermal contact resistances between the splat and the surfaces followed an inverse trend, with thermal contact resistance values increasing when the glass slides were roughened to 1.75 μm, and decreasing when the roughness was increased beyond 2.75 μm.

Impact on individual roughened glass slides, regardless of the surface temperature, produced splats with similar morphologies and maximum spread diameters. The splat cooling rates and the splat-substrate thermal contact resistances were approximately equal on the non-heated and heated rough surfaces. This suggested that the vaporization of adsorbates from the surfaces due to heating did not influence the spreading and cooling dynamics of the splat significantly. However, the micrometer average surface roughness played a larger role in determining the splat morphology, size, cooling rate, and splat-substrate thermal contact resistance. An increase in the splat cooling rates was observed as the surface roughness increased. This indicated that the physical contact between the splat and the glass surface increased as the splat liquid penetrated the spaces between the asperities on the highly roughened surfaces.

Acknowledgements The authors gratefully acknowledge the technical assistance of M. Lamontagne with assembly of the experimental apparatus and operation of the plasma-spraying equipment. The authors also thank General Electric Global Research for samples of textured silicon wafers and focused ion beam milling. Funding for this project was provided by the Natural Sciences and Engineering Research Council of Canada (NSERC).

References

1. Mehdizadeh N, Lamontagne M, Moreau C, Chandra S, Mostaghimi J (2005) J Thermal Spray Technol 14:354. doi:10.1361/105996305X59422
2. Shinoda K, Murakami H, Kuroda S, Oki S, Takehara K, Etoh T (2007) Appl Phys Lett 90:194103-1
3. McDonald A, Lamontagne M, Moreau C, Chandra S (2006) Thin Solid Films 514:212. doi:10.1016/j.tsf.2006.03.010
4. Fukumoto M, Nishioka E, Matsubara T (1999) Surf Coat Technol 120–121:131. doi:10.1016/S0257-8972(99)00349-7
5. Aziz S, Chandra S (2000) Int J Heat Mass Transfer 43:2841. doi:10.1016/S0017-9310(99)00350-6
6. Zhang H, Wang X, Zheng L, Jiang X (2001) Int J Heat Mass Transfer 44:4579. doi:10.1016/S0017-9310(01)00109-0
7. Shakeri S, Chandra S (2002) Int J Heat Mass Transfer 45:4561. doi:10.1016/S0017-9310(02)00170-9
8. Heichal Y, Chandra S (2005) J Heat Transfer 127:1269. doi:10.1115/1.2039114
9. Bianchi L, Leger A, Vardelle M, Vardelle A, Fauchais P (1997) Thin Solid Films 305:35. doi:10.1016/S0040-6090(97)80005-3
10. Sivakumar D, Katagiri K, Sato T, Nishiyama H (2005) Phys Fluids 17:100608-1. doi:10.1063/1.2033627
11. Shinoda K, Yamada A, Kambara M, Kojima Y, Yoshida T (2007) J Thermal Spray Technol 16:300. doi:10.1007/s11666-007-9033-8
12. McDonald A, Lamontagne M, Chandra S, Moreau C (2006) J Thermal Spray Technol 15:708. doi:10.1361/105996306X147027
13. Fantassi S, Vardelle M, Vardelle A, Fauchais P (1993) J Thermal Spray Technol 2:379. doi:10.1007/BF02645868
14. Vardelle M, Vardelle A, Leger A, Fauchais P, Gobin D (1994) J Thermal Spray Technol 4:50. doi:10.1007/BF02648528

15. Moreau C, Cielo P, Lamontagne M, Dallaire S, Vardelle M (1990) Meas Sci Technol 1:807. doi:10.1088/0957-0233/1/8/023
16. Gougeon P, Moreau C (2001) J Thermal Spray Technol 10:76. doi:10.1361/105996301770349538
17. Taylor J (1982) An introduction to error analysis: the study of uncertainties in physical measurements. University Science Books, p 89
18. Li L, Wang X, Wei G, Vaidya A, Zhang H, Sampath S (2004) Thin Solid Films 468:113. doi:10.1016/j.tsf.2004.05.073
19. Raessi M, Mostaghimi J, Bussmann M (2006) Thin Solid Films 506–507:133. doi:10.1016/j.tsf.2005.08.140
20. Pershin L, McDonald A, Chandra S (2006) Effect of substrate oxidation on the spreading of plasma-sprayed nickel. In: 3rd International conference on spray deposition and melt atomization, 3–6 September 2006, Universität Bremen, Bremen, Germany, 11 pages on compact disk
21. Dhiman R, McDonald A, Chandra S (2007) Surf Coat Technol 201:7789. doi:10.1016/j.surfcoat.2007.03.010
22. McDonald A, Moreau C, Chandra S (2007) Int J Heat Mass Transfer 50:1737. doi:10.1016/j.ijheatmasstransfer.2006.10.022
23. Pasandideh-Fard M, Qiao Y, Chandra S, Mostaghimi J (1996) Phys Fluids 8:650. doi:10.1063/1.868850
24. Jiang X, Wan Y, Hermann H, Sampath S (2001) Thin Solid Films 385:132. doi:10.1016/S0040-6090(01)00769-6
25. McDonald A, Moreau C, Chandra S (2007) Surf Coat Technol 202:23. doi:10.1016/j.surfcoat.2007.04.041
26. Moreau C, Bisson J, Lima R, Marple B (2005) Pure Appl Chem 77:443. doi:10.1351/pac200577020443
27. Syed A, Denoirjean A, Hannoyer B, Fauchais P, Denoirjean P, Khan A, Labbe J-C (2005) Surf Coat Technol 200:2317. doi:10.1016/j.surfcoat.2005.01.014